remote sensing

MDPI

Article

Fully Autonomous Orbit Determination and Synchronization for Satellite Navigation and Communication Systems in Halo Orbits

Gheorghe Sirbu and Mauro Leonardi *

Department of Electronic Engineering, University of Rome Tor Vergata, 00133 Roma, Italy
* Correspondence: mauro.leonardi@uniroma2.it

Abstract: This paper presents a solution for autonomous orbit determination and time synchronization of spacecraft in Halo orbits around Lagrange points using inter-satellite links. Lagrange points are stable positions in the gravitational field of two large bodies that allow for a sustained presence of a spacecraft in a specific region. However, a challenge in operating at these points is the lack of fixed landmarks for orbit determination. The proposed solution involves using inter-satellite links to perform range and range-rate measurements, allowing for accurate computation of the spacecraft's orbit parameters without the need for any facilities on Earth. Simulations using a fleet of three satellites in Near Rectilinear Halo Orbits around the Earth–Moon Lagrange point, proposed for the Lunar Gateway stations, were conducted to demonstrate the feasibility of the approach. The results show that inter-satellite links can provide reliable and accurate solutions for orbit determination with a DRMS error lower than one meter (90th percentile) and synchronization errors of around one nanosecond. This solution paves the way for a fully autonomous fleet of spacecraft that can be used for observation, telecommunication, and navigation missions.

Keywords: autonomous navigation; orbit determination; halo orbits, moon navigation

Citation: Sirbu, G.; Leonardi, M. Fully Autonomous Orbit Determination and Synchronization for Satellite Navigation and Communication Systems in Halo Orbits. *Remote Sens.* **2023**, *15*, 1173. https://doi.org/10.3390/rs15051173

Academic Editors: Antonio Genova and Sebastien Le Maistre

Received: 19 January 2023
Revised: 17 February 2023
Accepted: 19 February 2023
Published: 21 February 2023

1. Introduction

Missions to Lagrange points have been effective because they provide opportunities for flexible, low-energy trajectories. Lagrange points are equilibrium points in the space between two celestial bodies where the net gravitational force on an object at that point is zero. The five stable Lagrange points are L1, L2, L3, L4, and L5. In particular, L1 and L2 points are of interest because they offer a unique location in space where a spacecraft can maintain a stable position relative to the two celestial bodies. These points can be used for a variety of scientific and practical applications, such as satellite constellations, thermal observation, and studying the environment of celestial bodies.

Halo orbits and Near Rectilinear Halo Orbits (NRHO) are types of orbits that are related to Lagrange points. Halo orbits are defined by their proximity to a Lagrange point and their ability to remain in the vicinity of that point for an extended period of time, allowing for a broad range of scientific observations and technological applications. NRHO orbits are a specific type of Halo orbits that do not coincide with resonance with the motions of celestial bodies. These orbits are called "near-rectilinear" because they are close to being a straight line. NRHO orbits have the advantage of being less affected by the perturbations caused by other celestial bodies, making them useful for long-term missions.

One example of the application of this type of orbit is the James Webb Space Telescope (JWST or Webb), a joint NASA/ESA/CSA mission that launched an infrared-optimized 6.5 m space telescope in December 2021. The JWST will allow for a range of astronomical and cosmological studies, such as the observation of the first stars, the creation of the first galaxies, and a detailed analysis of potentially habitable exoplanets [1]. Another example is the Near-Earth Object Surveillance Mission (NEOSM), which is scheduled to be launched

by NASA in 2025. The NEOSM will use an infrared telescope to survey the solar system for potentially hazardous asteroids and will be conducted by the NEO Surveyor spacecraft, which will be stationed at the Sun–Earth L1 Lagrange point. This location allows it to look close to the Sun and detect objects inside Earth's orbit that would otherwise be difficult to spot from Earth or low Earth orbit [2].

Moreover, in recent years, several proposals have been made for using libration point orbits in the Earth–Moon system for communication and navigation services, particularly around the collinear L1 and L2 points. For example, Grebow et al. [3] have investigated the use of libration points for lunar South Pole coverage. Hamera et al. [4] analyzed the feasibility of using small satellites on Halo orbits for a lunar constellation. A lunar positioning system has also been designed using Lissajous [5] or Halo orbits [6] around both L1 and L2 points. Last, but not least, a future mission will deploy in a Moon Halo orbit, the Lunar Gateway: a space station that is a key part of NASA's Artemis program. The Lunar Gateway will serve as a science laboratory, a testing ground for new technologies, and a stepping stone for deep space exploration, including toward Mars.

For all these missions, and for future ones, Orbit Determination (OD) is a crucial element in order to meet the requirements and the goals of the missions. Conventionally, Earth-based tracking stations, such as the Deep Space Network (DSN), are used for tracking spacecraft. However, this practice has several limitations, especially if the number of simultaneous missions to be tracked increases. In fact, it has a capacity limit in terms of spacecraft that can be served simultaneously; it is costly and cannot support direct full coverage of a celestial object (for example, the case of spacecraft on the dark side of the Moon).

In recent years, a study introduced the Linked, Autonomous, Interplanetary Satellite Orbit Navigation (LiAISON) architecture as an alternative way for tracking spacecraft deployed in orbits around libration points, such as the Halo orbits. LiAISON is a concept of OD that uses relative inter-satellite measurements to estimate the absolute states of two or more spacecraft simultaneously [7].

An example of the use of this technique is the Cislunar Autonomous Positioning System Technology Operations and Navigation Experiment (CAPSTONE) mission [8]. It has started its operational activities, and it will serve as a pathfinder for navigation and operations in the same NRHO that will be utilized by NASA's Lunar Gateway. In addition to this objective, CAPSTONE contains a dedicated flight board for the Cislunar Autonomous Positioning System (CAPS), a framework for autonomous or near-autonomous navigation in cislunar space. The navigation architecture is based on inter-satellite radiometric data transferred between the CAPSTONE spacecraft, which is deployed in the NRHO orbit, and the Lunar Reconnaissance Orbiter (LRO), which is deployed in a low lunar orbit [9]. The combination of an Earth–Moon L2 Halo orbit and a low-lunar orbit has been shown to yield enough geometric and dynamic asymmetry such that the states of both spacecraft are observable.

The basic working principle proposed by the LiAISON study is based on the assumption that the Halo orbit has a unique size and shape because of the strong asymmetry of the three-body force field. This means that a spacecraft on these types of orbits can track a second spacecraft using inter-satellite measurements and determine their absolute positions and velocities without any Earth-based tracking or any other mathematical constraints.

In this work, we propose and evaluate, for a given case study, a method for Orbit Determination and Time Synchronization (OD&T) of spacecraft deployed in the same Halo orbit exploiting an inter-satellite link (ISL) for dual one-way measurements of the range and range rate between spacecraft. The proposed approach not only gives the possibility to have a fully autonomous orbit determination but also a total independent time synchronization of the spacecraft, avoiding the use of the DSN, which can be used only for periodic checks and calibrations.

For example, in the case of a single spacecraft mission, such as the JWST or any other scientific observation mission, exploiting only one spacecraft, additional small and low-cost

orbiters (called "floating anchors" hereafter) can be deployed from the same vector in the same orbit to perform the inter-satellite measurements to be used for autonomous OD. The mission's main spacecraft, exploiting the measurements (to and from the floating anchors), will be able to solve the OD problem autonomously and without any operation from the ground.

Moreover, for other types of missions, such as for navigation systems like the ones proposed in [10,11] or telecommunication systems in which, typically, more spacecraft are needed to cover a given region, the additional spacecraft can also be used to provide these services, being telecommunication relays to/from the Earth or other celestial bodies, or providing ranging signals for navigation purposes to other spacecraft or rovers. Finally, they can also be equipped, if needed, with instruments for remote sensing such as SAR, laser altimeters, or others, exploiting the precise orbit of the spacecraft.

After the description of the proposed OD and Timing procedure, the possible performances are evaluated for application in a NAV/COM constellation. In particular, in the case study, the possibility of adding two floating anchors to the Lunar Gateway, and to exploit this system of three spacecraft to deliver navigation and telecommunication signals to the Moon's South Pole, is investigated.

The paper is arranged as follows: in Section 2, the system concept and the inter-satellite measurements approach are introduced. In Sections 3 and 4, the Orbit Determination and Timing algorithms are explained in detail. Section 5 introduces and evaluates the case study, and discussions and conclusions follow in Section 6.

2. System Concept and Dual One-Way Measurements

As stated in the Introduction, there have been many missions that exploited Lagrange orbits because they offer a stable, convenient, and cost-effective location for missions that require a long-term presence in space or a fixed view of a particular region of the celestial sphere. In these particular orbits, it is possible to exploit relative tracking measurements to estimate relative and absolute orbit states for all participating spacecraft simultaneously if at least two spacecraft are deployed [7]. Usually, these measurements are conducted exploiting different communication bands such as X-band or K-band, or exploiting inter-satellite optical links.

In general, if the additional spacecraft are not used for other services, it can be assumed that only the main spacecraft have an onboard system able to process the measurements, allowing small, low complexity and cheap floating anchors, used for inter-satellite measurements. Figure 1 illustrates an example in which two spacecraft are deployed in a Lagrange orbit.

Different inter-satellite measurements can be performed by exploiting an ISL. The most used technique is the conventional two-way ranging that is also used by ground stations: it consists of sending an up-link signal coming from the TX-satellite (which could be a sequence of discrete tones or a pseudo-noise sequence); this signal is then received and re-transmitted back by the RX-satellite and received by the TX satellite, and this exchange allows the computation of the two-way propagation time [12]. Another technique is the telemetry-based ranging that provides a round-trip time derived from the telemetry stream [13,14]. This method does not require a return ranging signal, but it provides, as part of the telemetry stream, the delay between the acquired ranging signal and the start of the next telemetry frame. Both techniques provide a round-trip delay time solution at the signal source. Finally, an alternative technique is based on time transfer, as in the CCSDS Proximity-1 Space Link Protocol [15]: users can exchange epochs between satellites and derive the round-trip time using dedicated algorithms [16]. All of these techniques can be implemented, in principle, in any communication band, including the optical one. Finally, another effective way for two-way ranging can be the use of a satellite laser ranging technique exploiting retro-reflectors on the spacecraft [17].

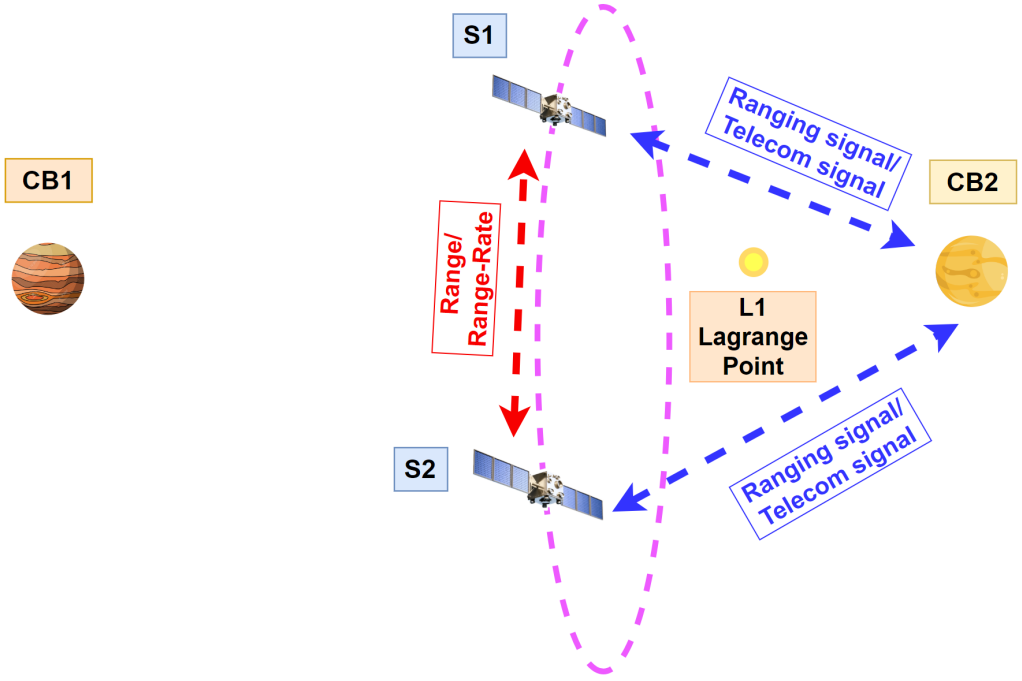

Figure 1. Illustrative example of inter-satellite measurements between two spacecraft deployed in an orbit around a Lagrange point.

In this work, the use of a different technique is proposed: the so-called dual one-way. It has the advantage of producing not only an estimation of the satellite range but also an estimation of the satellite clock biases.

Referring to Figure 2, each spacecraft is equipped with a transmitter and a receiver to exchange ranging signals and with a reference clock to measure the Time of Transmission and the Time of Arrival of these signals. The working principle is mutated from the one used in GNSS: pseudo-random codes are transmitted from one spacecraft and received in the other exploiting a Delay Lock Loop (DLL) to measure the signal Time of Arrival (TOA) and a Phase Lock Loop (PLL) to measure the signal Doppler shift (Frequency Of Arrival-FOA). These measurements are used to estimate the range, the range rate, and the clock bias at regular time intervals (ΔT); the measurements are then accumulated for a given time span (T) and used to solve the OD&T problem in the main spacecraft.

The orbiting spacecraft exchange data and measurements exploiting the ISL and, if they have a precise OD&T, can be used to transmit to the celestial body Navigation and Telecommunication signals.

In more detail, the range between two satellites is defined as the linear distance between the spacecraft and can be measured by exploiting the Time Of Arrival (TOA), if the TOA measurements taken on the anchors are transmitted back to the main spacecraft. In detail, let us have two spacecraft i and j in position $\mathbf{r}_i = (x_i, y_i, z_i)^T$ and $\mathbf{r}_j = (x_j, y_j, z_j)^T$ and let us assume a common reference time t. The spacecraft can have different clock biases with respect to the reference time; δt_i, δt_j, and the time of flight of signal can be measured by the use of the TOAs taken by both of the satellites, in the following way:

$$(TOA_i - ToT_j) = \frac{\rho_{i,j}}{c} = \frac{\|\mathbf{r}_i - \mathbf{r}_j\|}{c} + (\delta t_i - \delta t_j) + \epsilon_{i,j} \tag{1}$$

$$(TOA_j - ToT_i) = \frac{\rho_{j,i}}{c} = \frac{\|\mathbf{r}_j - \mathbf{r}_i\|}{c} + (\delta t_j - \delta t_i) + \epsilon_{j,i} \tag{2}$$

where ToT_j is the Time of Transmission on satellite j (encoded in the transmitted signal), and $\rho_{i,j}$ is called "pseudorange" from satellite i to satellite j.

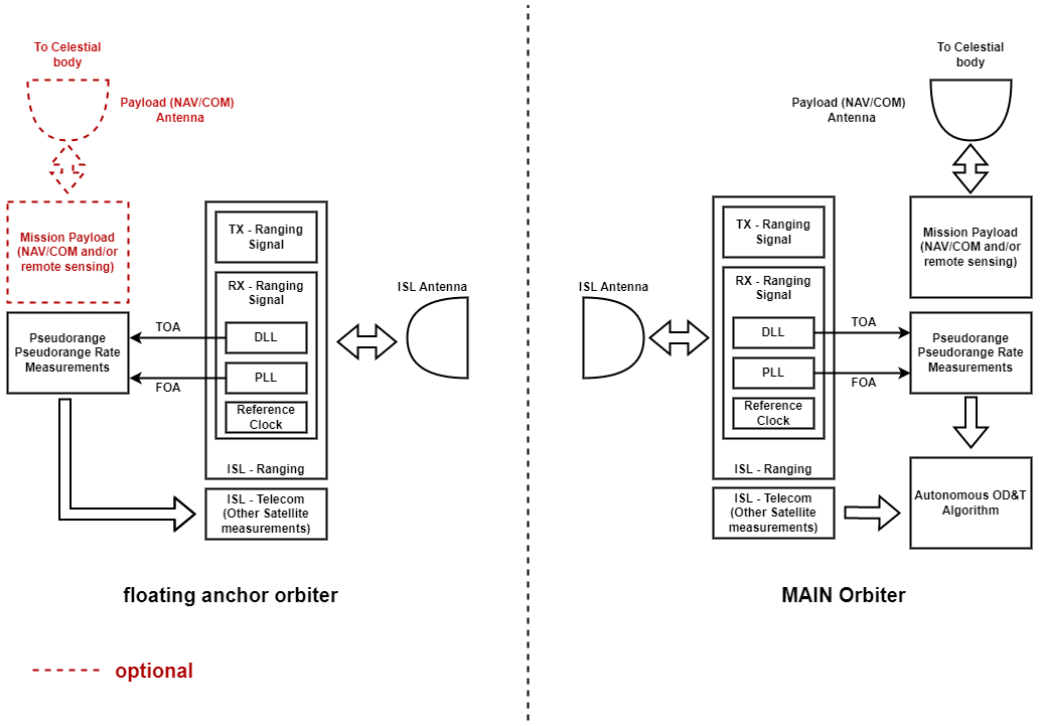

Figure 2. Block diagram of the proposed main orbiter and floating anchors.

Finally, $\epsilon_{i,j}$ is the measurement error. The pseudo-ranges, $\rho_{i,j}$ and $\rho_{j,i}$ do not coincide with the real range, but, if both of the spacecraft produce a measurement, it is possible to compute the range making the average of the two pseudo-ranges because, by definition, $(\delta t_i - \delta t_j) = -(\delta t_j - \delta t_i)$:

$$r_{i,j} = \|\mathbf{r}_i - \mathbf{r}_j\| = \frac{\rho_{i,j} + \rho_{j,i}}{2} + \frac{c(\epsilon_i + \epsilon_j)}{2} \tag{3}$$

Moreover, if the difference between the pseudo ranges also computed, an estimation of the clock bias between the two spacecraft can be obtained:

$$\delta t_{i,j} = \delta t_i - \delta t_j = \frac{\rho_{i,j} - \rho_{j,i}}{2c} + \frac{(\epsilon_{i,j} - \epsilon_{j,i})}{2} \tag{4}$$

As mentioned before, the time of arrival is measured in the receiver exploiting a Delay Locked Loop as in the case of GNSS [18].

Exploiting the same signals, it is also possible to measure the range rate between two spacecraft, with i and j exploring the Doppler effect. Let us recall that the Doppler shift for a radio frequency signal is given by:

$$f_d = -(\delta v)/c \cdot f_0 \tag{5}$$

where δv is the radial velocity of the spacecraft j with respect to the spacecraft i, c is the speed of light, and f_0 is the carrier frequency of the data link. It follows that δv can be seen as the derivative of the geometrical distance of the satellites and that the Doppler shift can be expressed as follows:

$$f_{i,j} = \frac{c}{f_0} \cdot \dot{\rho}_{i,j} = \frac{c}{f_0} \cdot \left(\frac{[(x_i - x_j)(\dot{x}_i - \dot{x}_j] + [(y_i - y_j)(\dot{y}_i - \dot{y}_j)] + [(z_i - z_j)(\dot{z}_i - \dot{z}_j]}{r} \right) + n_{i,j} \tag{6}$$

where $n_{i,j}$ represents the measurement error in measuring the Doppler shift of satellite i from satellite j. The Doppler shift can be measured by the Phase Lock Loop implemented in the receivers [18].

Concerning the measurement errors, measuring the TOA of a given signal is a well-known problem, and various methods have been proposed in the literature to find the Cramer–Rao limit, and the most used expression is given by [19]:

$$\sigma_{TOA} \cong \frac{1}{\beta\sqrt{2E/N_0}} \tag{7}$$

where E is the signal energy, N_0 is the noise power spectral density, and β is the Gabor bandwidth, which is defined as:

$$\beta^2 = \frac{\int_{-\infty}^{+\infty}(2\pi f)^2\left|S(f)\right|^2 df}{\int_{-\infty}^{+\infty}\left|S(f)\right|^2 df} \tag{8}$$

where $S(f)$ is the power spectrum of the received signal.
In the same manner, a similar expression can be formulated for the measurement of the Frequency of Arrival (FOA) of the signal [19]:

$$\sigma_{FOA} \cong \frac{1}{\alpha\sqrt{2E/N_0}} \tag{9}$$

where α is the effective duration, which is defined as [19]:

$$\alpha^2 = \frac{\int_{-\infty}^{+\infty}(2\pi t)^2\left|s(t)\right|^2 dt}{\int_{-\infty}^{+\infty}\left|s(t)\right|^2 dt}, \tag{10}$$

where $s(t)$ is the received signal.

In the case of pseudo-random code and Delay Look Loop (DLL), the TOA error model can also be refined by taking into account many of the receiver and signal parameters, by the following expression [18]:

$$\sigma_{DLL} \approx \begin{cases} \sqrt{\frac{B_n}{2C/N_0}D\left[1+\frac{2}{T_{int}C/N_0(2D)}\right]}, & D \geq \frac{\pi R_c}{B_{fe}} \\ \sqrt{\frac{B_n}{2C/N_0}\left(\frac{1}{B_{fe}T_c}+\frac{B_{fe}T_c}{\pi-1}\left(D-\frac{1}{B_{fe}T_c}\right)^2\right)\left[1+\frac{2}{T_{int}C/N_0(2D)}\right]}, & \frac{R_c}{B_{fe}} < D < \frac{\pi R_c}{B_{fe}} \\ \sqrt{\frac{B_n}{2C/N_0}\left(\frac{1}{B_{fe}T_c}\right)\left[1+\frac{1}{T_{int}C/N_0}\right]}, & D \leq \frac{R_c}{B_{fe}} \end{cases} \tag{11}$$

where B_n is the code loop noise bandwidth, B_{fe} is the double-sided front-end bandwidth, T_{int} is the predetection integration time, T_c is the chip period, $R_c = 1/T_c$ is the spreading code rate, C/N_0 is the carrier to noise power ratio, and D is the early-to-late correlator spacing.

Moreover, Ref. [20] demonstrates that using the PLL filter to estimate the Doppler frequency and the range rate gives the following error due to thermal noise (for the range rate):

$$\sigma_{PLL} = \frac{\lambda_c}{2\pi T_{int}}\sqrt{\frac{B_d}{C/N_0}\left[1+\frac{1}{2T_{int}C/N_0}\right]} \tag{12}$$

where λ_c is the wavelength of the signal, T_{int} is the coherent integration time, C/N_0 is the carrier to noise ratio, and B_d is the Doppler bandwidth defined as:

$$B_d = \frac{1}{2}\int_{-0.5/T_{int}}^{0.5/T_{int}} |H_{nf}(e^{j2\pi f T_{int}})|^2\, df \tag{13}$$

where H_{nf} is the frequency noise impulse responses transformed into the Z-domain. The Doppler bandwidth B_d summarizes in a single parameter the ability of the tracking loop to produce smooth frequency estimates.

Having these formulations, it is possible to find the range and range-rate measurement errors knowing the receiver and signal parameters. Referring to the literature, in [21], the range measurement error between GPS satellites is assumed to be 1 m by using ranging measurementswith a maximum ranging distance of 50,000 km; Ref. [22] proposes a method for relative navigation for microsatellites using inter-satellite measurements, and the range error is assumed to be at a maximum of 10 cm for a maximum ranging distance of 10 km. Another example can be found in [23], where a precise ranging and time synchronization system was implemented based on dual one-way ranging with a precision of the ranging measures of 1.038 m. Ref. [24] proposes a solution for relative OD using inter-satellite range measurements, and the ranging measurement error is assumed to be Gaussian with a standard deviation of 1 m.

Refs. [18,25,26] explain in more detail the range measurement assumptions and the relative models, and it is shown that the measurement error always depends on the carrier-to-noise ratio, C/N_0, remaining below 1 m for most cases.

Concerning the range rate, in [27], the measurement accuracy is assumed to be 0.01 mm/s, and in [28], an autonomous navigation system for satellites deployed in Martian orbits was proposed, and the worst accuracy in range rate was assumed to be below 4 µm/s. The inter-satellite link, in this case, was in the X-band, and the Carrier-to-Noise ratio was assumed to be equal to 30 db-Hz.

In this work, we assume the use of the Ka-band

($f_c = 26$ GHz) for the inter-satellite link. It is compliant with the standards defined in [29], allowing a range error of 1 m, obtained, for example, with a typical DLL code noise bandwidth B_n of 0.2 Hz, an integration time T of 1 s and $C/N_0 = 35$ dB-Hz, with the following other typical parameters: $B_{fe} = 8$ MHz, $R_c = 2.046$ Mcps, and $D = 0.488$ µs.

The range-rate error is assumed to be below 0.06 mm/s, and it can be obtained with the PLL with a Doppler bandwidth B_d of 1 Hz, an integration time T_{int} of less than five seconds, and a carrier-to-noise ratio C/N_0 of 35 dB-Hz.

In the following sections, the proposed method to use these measurements for a precise OD&T is reported.

3. Orbit Determination with ISL Measurements

Let us assume to have a system of $N > 1$ orbiters in a Halo orbit. This system can be easily described by exploiting the Circular Restricted Three-Body Problem (CRTBP) where two massive bodies are considered orbiting around their mutual center of mass, and the spacecraft with infinitesimal masses experience forces due to the gravitational influence of both bodies simultaneously. All the bodies are approximated as point masses. Moreover, to simplify the notation, let us assume to use a reference frame centered in the two celestial body center of gravity and keep the x-axis pointed towards the second celestial body, obtaining a frame rotating with constant angular velocity, equal to the mean motion of the system.

Finally, let us scale the system in such a way that the distance between the two main bodies, as well as the angular velocity, are set to 1 (see Figure 3).

In this coordinate frame, it is possible to define the state vector for any spacecraft (containing its position and velocity) as:

$$\boldsymbol{X} = [X, Y, Z, \dot{X}, \dot{Y}, \dot{Z}]^T \tag{14}$$

or, in the general case of N spacecraft as:

$$\boldsymbol{X} = [X_1, Y_1, Z_1, \dot{X}_1, \dot{Y}_1, \dot{Z}_1, \ldots, X_N, Y_N, Z_N, \dot{X}_N, \dot{Y}_N, \dot{Z}_N] \tag{15}$$

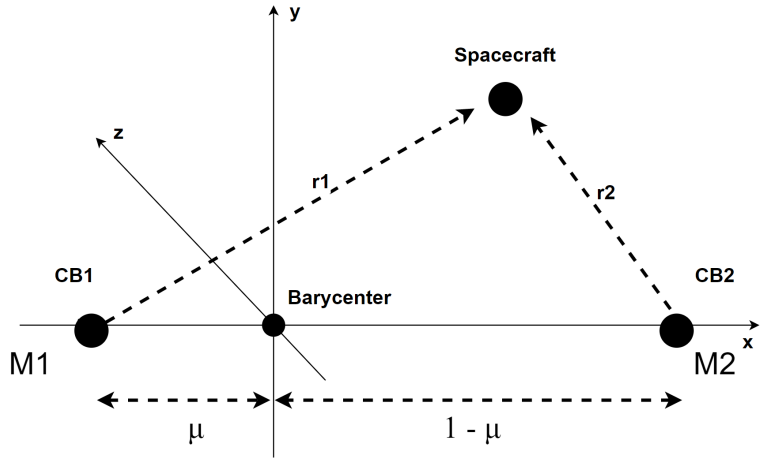

Figure 3. The reference frame used to solve the OD problem.

Moreover, in this reference frame for the generic spacecraft i, the equations take the following form: [30]:

$$\begin{aligned} \ddot{X}_i &= \frac{\partial U_i}{\partial X_i} + 2\dot{Y}_i \\ \ddot{Y}_i &= \frac{\partial U_i}{\partial Y_i} - 2\dot{X}_i \\ \ddot{Z}_i &= \frac{\partial U_i}{\partial Z_i} \end{aligned} \tag{16}$$

where U_i is the potential function:

$$U_i = (X_i^2 + Y_i^2)/2 + (1-\mu)/d_{1,i} + \mu/d_{2,i} \tag{17}$$

and

$$\begin{aligned} \mu &= m_2/(m_1+m_2) \\ d_{1,i} &= \sqrt{(X_i+\mu)^2 + Y_i^2 + Z_i^2} \\ d_{2,i} &= \sqrt{(X_i+\mu-1)^2 + Y_i^2 + Z_i^2} \end{aligned} \tag{18}$$

and m_1 and m_2 are the celestial body masses.

In this particular frame, a batch-weighted least square orbit determination algorithm [30] can be used to estimate the initial state of all the spacecraft.

The differential equation of the satellite motion, $\dot{\boldsymbol{X}} = \mathbf{F}(\mathbf{X}, t)$, can be derived from the motion law and can be used to propagate the initial state to any possible time t by integration. It follows that, knowing the initial state of the system, it is possible to derive the state, $\mathbf{X}(t)$, for any possible time t.

In the same way, having a reference solution (that is a guess with an error of the initial state), it is possible to also compute a reference state for the time t, $\mathbf{X}^*(t)$.

Finally, for any time t, it is also possible to define the expected measurement vector $\mathbf{Y}^*(t)$ for the reference solution and the real measurement vector for $\mathbf{Y}(t)$. The vector $\mathbf{Y}(t)$ contains the set of the range and range-rate measurements taken at time t as defined in Equation (3) and in Equation (6). Making the hypothesis conduct the measurement process with an update time of Δt for a Time span of T, it is possible to compute the state deviation, $\mathbf{x}(t_k)$, and the observation residual, $\mathbf{y}(t_K)$, for each measurement instant $k = 1 \ldots M$:

$$\mathbf{x}(t_k) = \mathbf{X}(t_k) - \mathbf{X}^*(t_k) \tag{19}$$

$$\mathbf{y}(t_k) = \mathbf{Y}(t_k) - \mathbf{Y}^*(t_k) \tag{20}$$

The state deviations, $\mathbf{x}(t_k)$, can be mapped back to the initial epoch, t_0, with the state transition matrix, $\mathbf{\Phi}$, as follows:

$$\mathbf{x}(t_k) = \mathbf{\Phi}(t_k, t_0)\mathbf{x}(t_0) \tag{21}$$

The state transition matrix is obtained by numerical integration, and its differential function is:

$$\dot{\mathbf{\Phi}}(t_k, t_0) = \mathbf{A}(t_k)\mathbf{\Phi}(t_k, t_0) \tag{22}$$

where:

$$\mathbf{A}(t_k) = [(\partial \mathbf{F}(\mathbf{X}^*, t_k))/(\partial \mathbf{X}(t_k))]^* \tag{23}$$

where $[]^*$ means computed on the reference trajectory.

Considering the case of N spacecraft, $\mathbf{A}$ has the following formulation $\mathbf{A} = diag(\mathbf{A}_1, \ldots, \mathbf{A}_N)$, where:

$$A_i = \begin{bmatrix} 0 & 0 & 0 & 1 & 0 & 0 \\ 0 & 0 & 0 & 0 & 1 & 0 \\ 0 & 0 & 0 & 0 & 0 & 1 \\ \partial^2 U_i/\partial^2 X & \partial^2 U_i/(\partial X \partial Y) & \partial^2 U_i/(\partial X \partial Z) & 0 & 2 & 0 \\ \partial^2 U_i/(\partial Y \partial X) & \partial^2 U_i/(\partial^2 Y) & \partial^2 U_i/(\partial Y \partial Z) & -2 & 0 & 0 \\ \partial^2 U_i/(\partial Z \partial X) & \partial^2 U_i/(\partial Z \partial Y) & \partial^2 U_i/(\partial^2 Z) & 0 & 0 & 0 \end{bmatrix} \tag{24}$$

The same approach can be used to map back all the measurements to the initial time t_0, exploiting the observation residuals, defining the $\hat{\mathbf{H}}$ matrix as:

$$\hat{\boldsymbol{H}} = [\partial \boldsymbol{G}/\partial \boldsymbol{X}]^* \tag{25}$$

where $\boldsymbol{G}$ is the function that relates the observations to the state vector in the following way:

$$\boldsymbol{Y} = \boldsymbol{G}(\boldsymbol{X}, t) + \boldsymbol{\epsilon} \tag{26}$$

as given in Equations (3) and (6).

Therefore, it is possible to move the set of observations at time t_k back to the initial epoch t_0 defining the matrix $\boldsymbol{H}_k$:

$$\boldsymbol{H}_k = \hat{\boldsymbol{H}}\mathbf{\Phi}(t_k, t0) \tag{27}$$

When the total number of observations is larger than the number of unknowns, a solution for $\mathbf{x}(t_0)$ can be found by exploiting the normal equation:

$$\boldsymbol{\Lambda x} = \boldsymbol{N} \tag{28}$$

where $\boldsymbol{\Lambda} = \boldsymbol{H}^T \boldsymbol{W} \boldsymbol{H}$ is the information matrix, and $\boldsymbol{N} = \boldsymbol{H}^T \boldsymbol{W} \boldsymbol{y}$ is the reduced residual vector, where $\mathbf{H}$ is the block matrix containing the observation–state relationship matrices $\boldsymbol{H}_k$ for all the epochs, and is given by:

$$\mathbf{H} = \begin{bmatrix} \mathbf{H}_1 \\ \vdots \\ \mathbf{H}_N \end{bmatrix} \tag{29}$$

and $\mathbf{W}$ is the weighting matrix:

$$\boldsymbol{W} = \begin{bmatrix} W_1 & \dots & 0 \\ & \ddots & \\ 0 & \dots & W_l \end{bmatrix} \tag{30}$$

assuming that the observation errors can be modeled as white Gaussian noise, and the standard deviation in the observation noise can be denoted as σ_p, $W_p = 1/\sigma_p$.

4. Satellite Synchronization

As introduced before, by exploiting the dual one-way technique, it is possible to compute the clock bias between the two spacecraft at the time of the measurement.

Unfortunately, computing only the time bias for a given specific time is not sufficient to model the deviation between two clocks. A more complex model that considers deterministic and random components of the clock deviation, such as bias, drift, and drift rate, is usually needed. A common solution is the use of stochastic differential equations.

The clock time and frequency errors for a time epoch k can be derived from the previous one by exploiting, for example, the model proposed in [31] where two main clock noises are considered: White Frequency Modulation (WFM) and Random Walk Frequency Modulation (RWFM). These two noises generate on the clock's phase a Wiener noise (integral of the WFM) and an integrated Wiener noise (integral of the RWFM):

$$X_1(t_{k+1}) = X_1(t_k) + (X_2(t_k) + \mu_1)\tau + \mu_2 \frac{\tau^2}{2} + J_{k,1} \tag{31}$$

$$X_2(t_{k+1}) = X_2(t_k) + \mu_2 \tau + J_{k,2} \tag{32}$$

$$\boldsymbol{J}_k \sim \mathcal{N}\left(0, \begin{bmatrix} \sigma_1^2 \tau + \sigma_2^2 \frac{\tau^3}{3} & \sigma_2^2 \frac{\tau^2}{2} \\ \sigma_2^2 \frac{\tau^2}{2} & \sigma_2^2 \tau \end{bmatrix}\right) \tag{33}$$

where X_1 represents the clock phase deviation (time Bias), X_2 represents the clock frequency deviation, and μ_1 and μ_2 are the clock deterministic drift terms. The vector $\boldsymbol{J}_k$ is a bivariate random variable with zero mean and variance that depends on two parameters: σ_1, which is the diffusion coefficient of the phase noise, and σ_2, which is the diffusion coefficient of the frequency noise; it represents the covariance matrix of the error related to the specific clock. By setting the μ_1, μ_2, σ_1, and σ_2, it is possible to set the noise model representing the desired type of clock to be represented for a long time.

For short-time modeling, this model can be replaced by a simpler one that takes into account only the deterministic components of the clock deviation, which are the time bias, the drift, and the drift rate using the following polynomial representation for the bias of each satellite clock at given epoch (t_0) [32,33]:

$$\delta t = a_0 + a_1(t - t_0) + a_2(t - t_0)^2 \tag{34}$$

where a_0 is the clock offset, a_1 is the clock drift, and a_2 is the clock drift rate. This simpler model is commonly used to represent the clock error in the GNSS system and can be accurate enough to represent the clock error if it is frequently updated. For example, in the GPS system, the parameters of the clock are updated every two hours [34].

In this work, this second approach is proposed and, considering the main spacecraft clock as the reference one, the clock parameters to compute the bias with respect to the main spacecraft for the anchor satellite i can be collected in the vector $\mathbf{a}_i = \left[a_0^i, a_1^i, a_2^i\right]$.

Recalling that, for each time epoch t_k, the TOA measurements are able to produce an estimation of the time bias $\delta t(t_k)$ between the spacecraft clocks as derived in Equation (4),

for each spacecraft, it is possible to estimate a_0^i, a_1^i, a_2^i by linear regression or a Least Square solution, inverting the system of equations:

$$\begin{cases} \delta t_i(t_1) & = a_0^i + a_1^i(t_1 - t_0) + a_2^i(t_1 - t_0)^2 + \epsilon(t_1) \\ & \vdots \\ \delta t_i(t_k) & = a_0^i + a_1^i(t_k - t_0) + a_2^i(t_k - t_0)^2 + \epsilon(t_1) \\ & \vdots \\ \delta t_i(t_K) & = a_0^i + a_1^i(t_K - t_0) + a_2^i(t_K - t_0)^2 + \epsilon(t_1) \end{cases} \tag{35}$$

where K is the number of epochs used for the estimation.

It must be noted that, as mentioned before, the proposed model works for a short time, and it is not possible to use the estimated parameters a_0, a_1, a_2 for long periods: the parameter estimation must be repeated, after a given time, for example, every 2 or 3 h.

It follows that the Time Synchronization and Orbit Determination processes, also if based on the same set of measurements, may have the same renewal time (Δt) but different time spans.

In Figure 4, a schematic representation of the whole algorithm is reported. Every Δt, a set of TOA and FOA measurements, is taken and collected from the main spacecraft. The measurements are used to derive the range, range rate, and clock biases between spacecraft. At the time t_k, the range and range rate accumulated from the last epochs in T_{span} are used to derive the state deviation and the measurement residuals. Having all the epochs of the selected time span, the normal equation can be solved and the state of the spacecraft at time t_0 can be estimated. In the same way, the clock parameters for the epoch t_1 are estimated with the last M_K epochs. After that, the orbits and clocks parameters can be used to propagate the satellite's position and time to the future epochs, and the sliding windows can be moved to the epoch t_{k+1}.

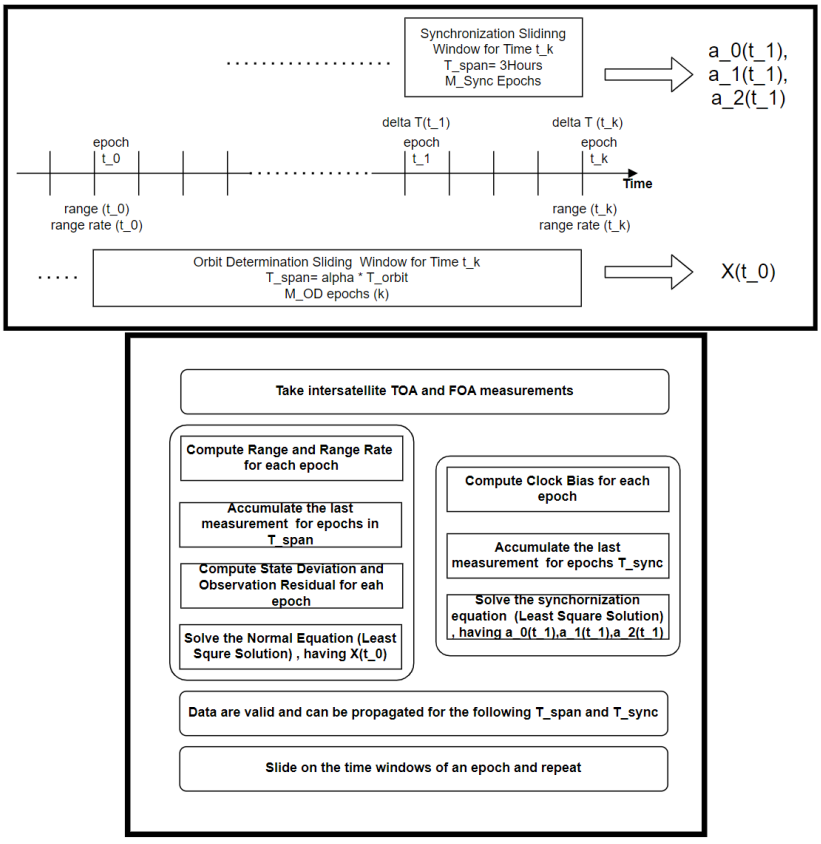

Figure 4. Schematic representation of the Orbit Determination and synchronization algorithms.

5. Evaluation for Lunar NHRO Orbiters for NAV/COM Applications

One of the next missions that will be deployed in a Moon Halo orbit is the Lunar Gateway. The Lunar Gateway will be a science laboratory, a test bed for innovative technologies, and represents a stepping stone to deep space exploration, especially toward Mars [9]. The current baseline orbit for the Gateway is an NRHO with a period of approximately 6.56 days. It exhibits a 9:2 resonance with the lunar synodic period, completing nine revolutions around the Moon every two synodic months. The mean radius at perilune is approximately 3400 km, while the orbit extends to a radius of approximately 71,000 km at apolune [35].

The case study proposed and evaluated here is a system of three spacecraft: the main one, which can be the Gateway, and two additional anchor orbiters for a totally autonomous and precise OD&T and for providing Navigation and Telecommunication services on the Moon's surface, and in particular on the Moon South Pole, where the future Artemis missions are planned [36].

The idea is to test the possibility to add a reduced number of small and inexpensive spacecraft in the same orbit as the Lunar Gateway to be used as relays for communication with the Moon's Surface and for the transmission of ranging signals (as in the case of terrestrial GNSS system) to provide a navigation service. The additional orbiters can be equipped only with a telecommunication payload for communication with the Moon's surface (and for transmitting ranging signals) and with ISLs able to perform the TOA and FOA measurements with the Gateway and, in principle, can be deployed from the same vector used for the Gateway components or from the Gateway itself. All of the OD&T operations are performed on the Gateway.

The constellation for the test is composed of the Gateway and two additional spacecraft and is represented in Figure 5; all the details about the constellation are reported in Table 1.

As can be seen from Figure 5, the spacecraft are not equally distributed in the orbit; this configuration was chosen because it has good performance in terms of Navigation and Telecommunication service availability on the South Pole of the Moon. Figure 6 reports the elevation angle for each spacecraft for all the orbiting period, for different epochs, as seen from the South Pole. It is possible to note that there is always at least one satellite in the view from the South Pole that can be used for telecommunication purposes with an elevation angle higher than 40 degrees.

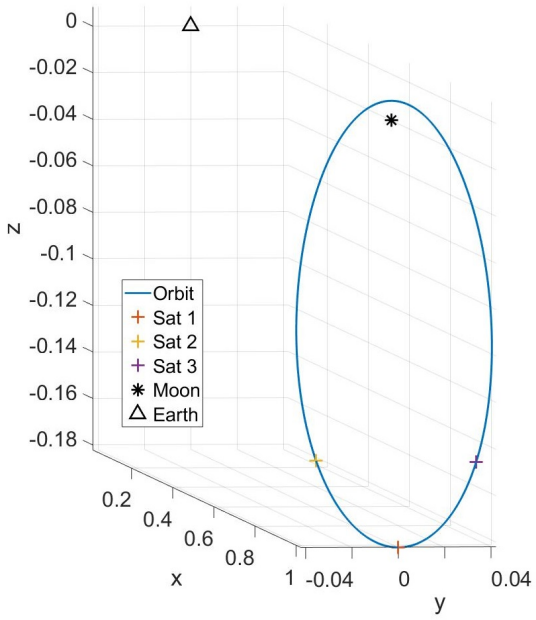

Figure 5. Constellation of spacecraft in the NRHO, composed of the Lunar Gateway and two additional floating anchors.

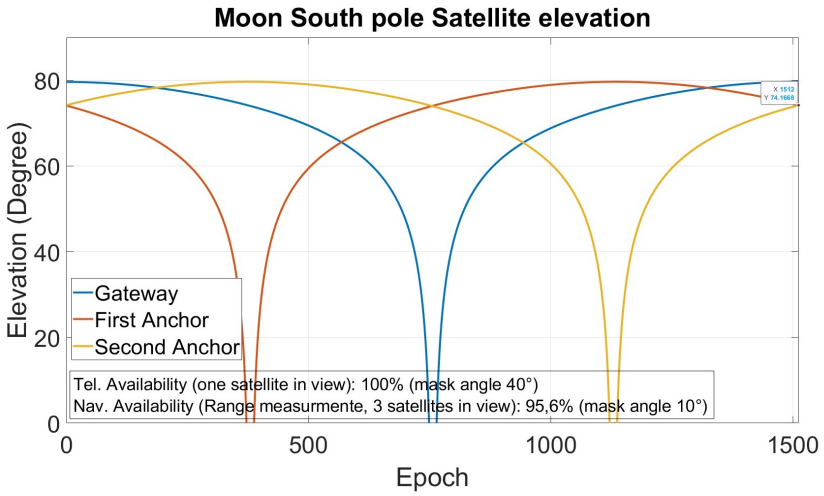

Figure 6. Elevation angle of the Lunar Gateway and the two anchors with respect to a user located at the Moon South Pole.

Table 1. Reference Orbit and spacecraft initial condition for the spacecraft used in the simulation. The orbit period is referred to the normalized CRTBMP frame. For the Earth–Moon system, the time normalization constant is $t^* = 4.3644$ days.

Parameter	Value
Orbit type	9:2 lunar synodic resonance
Orbit Period	6.59 days
Perilune Radius	3196–3557 km
Apolune Radius	70,000 km
Orb.Period (non-dimensional units)	1.5112
$[x_0^1, y_0^1, z_0^1, \dot{x}_0^1, \dot{y}_0^1, \dot{z}_0^1]$	[1.0221, 0, −0.1821, −0, −0.1033, 0]
$[x_0^2, y_0^2, z_0^2, \dot{x}_0^2, \dot{y}_0^2, \dot{z}_0^2]$	[1.01282, −0.03468, −0.14507, −0.04860, −0.06772, 0.20422]
$[x_0^3, y_0^3, z_0^3, \dot{x}_0^3, \dot{y}_0^3, \dot{z}_0^3]$	[1.01284, 0.03442, −0.14582, 0.04809, −0.06846, −0.20189]

Moreover, three satellites are in view for more than 95% of the time with an elevation angle higher than 10 degrees and can be used as ranging sources for navigation purposes. Having three synchronized satellites in view, it is possible to have an estimation of the user position if it is imposed to be on the Moon surface exploiting a Digital Elevation Model (DEM) or, for flying users, exploiting the DEM together with an altimeter as shown, for example, in [37].

Simulations of the OD&T process are performed using the previously introduced orbit determination algorithm and considering the errors reported in Table 2, exploding different time spans (between one and two orbital periods) and measuring intervals (between 15 and 60 min) for two system conditions: with (RR) and without (NORR) range-rate measurements. These two different configurations are compared to understand if the simpler configuration exploiting anchors without the ability to perform PLL-based range-rate measurements is also able to allow OD&T performances compatible with the stringent requirements to provide a navigation service.

Regarding the measurement errors reported in Table 2, they are the typical measurement performances that can be obtained using a receiver implementing DLL and PLL and referring to Equations (11) and (12) with the previously mentioned parameters.

Monte Carlo runs were carried out with an initial error on the reference orbit generated for each run with a Gaussian distribution, zero mean, and a standard deviation of 100 m for the position error and 0.1 mm/s for the velocity error. The error on the inter-satellite range measurements was considered Gaussian distributed with 1 m of standard deviation for each measurement session, and the error on the range rate is considered with a standard deviation of 0.06 mm/s.

Table 2. Parameters used for the performance evaluation.

Parameters	Value
Inter-spacecraft Range error (std)	1 m
Inter-spacecraft Range-Rate error (std)	0.06 mm/s
Measurements Interval	15–30–60 min
Time Span for OD	1–1.5–2 T (T = 6.59 days)
Time Span for Sync	3 h
Reference Orbit Position error (std)	100 m
Reference Orbit Velocities error (std)	1 mm/s

To evaluate the performance of the Orbit Determination process, the Distance Root Mean Square (DRMS) of the estimated trajectories with respect to the nominal one was computed: the estimated, $\mathbf{X}_l^e$, and the nominal, $\mathbf{X}_l$, trajectories were propagated for three hours, and the norm of the displacement vector (distance) for each epoch is used to compute the DRMS for the given spacecraft:

$$DRMS_m = \sqrt{\sum_{t_{span}} e_i^2} \tag{36}$$

$$e_l = \|\mathbf{X}_l - \mathbf{X}_l^e\| \tag{37}$$

where m indicates the m-th satellite, and l indicates the epoch of the propagation. Finally, the average of the DRMS error for all the spacecraft (Gateway and anchors) was considered:

$$DRMS_{mean} = \sum_j DRMS_j / N_{spacecraft} \tag{38}$$

For comparison, a classic orbit determination process exploiting an Earth-based measuring station performing the same measurements (range and range rate) was also simulated for the same time spans and measurement rate (measurements are taken only from the ground, without the use of any ISL).

Examples of results for a time span of 9.89 days (1.5 T) and measurement time interval of 30 min are reported in Figures 7 and 8, where the histograms for the DRMS orbit error (in meters) for 500 Monte Carlo runs are reported for the two cases: with and without the range-rate measurements, respectively, and compared with the ground-based approach. It is possible to note that, with this configuration, the obtained performance is similar to the one obtained with the classical Earth-based OD method. Moreover, the results show that sub-meter positional DRMS error can be obtained by the use of range and range-rate measurements with a totally autonomous approach.

In Table 3, the 90th percentile for the DRMS errors computed for different simulations, varying the time span and measurement intervals, are reported. Apart from the first value of the time span, the proposed Autonomous OD gives similar or better results than the OD from the Earth and with a sub-meter DRMS error for a large part of the tested cases.

Concerning the synchronization, the performances are calculated with the same approach: the clock was propagated with the nominal and estimated parameters, and the RMS clock bias was computed for different epochs in a time span of three hours.

The obtained results are compared with the a posteriori synchronization method based on GPS satellites proposed in [38] in which, after an independent orbit determination, the GPS satellites are used for Time Transfer to the Moon orbiting spacecraft.

To mitigate the simplified clock model errors, the time span for estimating the clock parameters was chosen to be equal to 3 h.

In addition, in this case, the results are encouraging and always better than the ones obtained in [38]. Figures 9 and 10 report the histograms of the RMS error for 500 Monte Carlo runs with and without RR measurements, compared with the method proposed in [38].

Table 3. 90th percentile of the DRMS position error (in meters) for different time spans and measurement rates int and measurement time span, T_s.

Earth ODT Position-DRMS Error in Meters (90th Percentile)						
	NORR			**RR**		
int/T_s	**15 min.**	**30 min.**	**60 min.**	**15 min.**	**30 min.**	**60 min.**
6.59 days (1 T)	1.97	2.86	3.96	0.74	1.01	1.44
9.89 days (1.5 T)	1.05	1.49	2.15	0.32	0.46	0.66
13.2 days (2 T)	0.67	0.94	1.32	0.23	0.33	0.45
Autonomous ODT Position-DRMS Error in Meters (90th Percentile)						
	NORR			**RR**		
int/T_s	**15 min.**	**30 min.**	**60 min.**	**15 min.**	**30 min.**	**60 min.**
6.59 days (1 T)	5.74	8.14	11.80	3.77	5.71	7.78
9.89 days (1.5 T)	0.96	1.29	1.81	0.49	0.67	1.00
13.2 days (2 T)	0.32	0.46	0.62	0.21	0.30	0.43

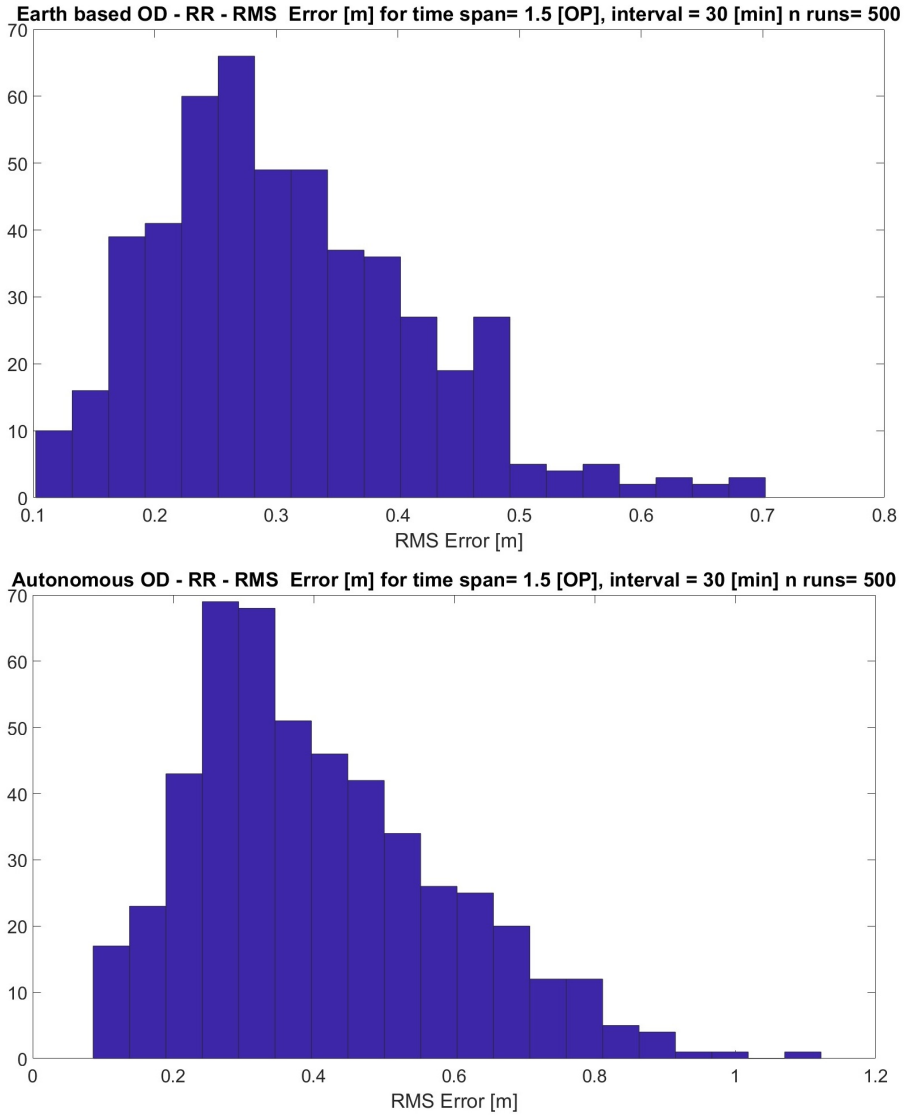

Figure 7. Histograms for the rms orbit error with 500 Monte Carlo runs, using range and range-rate measures, (**top**) Earth-based OD, (**bottom**) Autonomous OD.

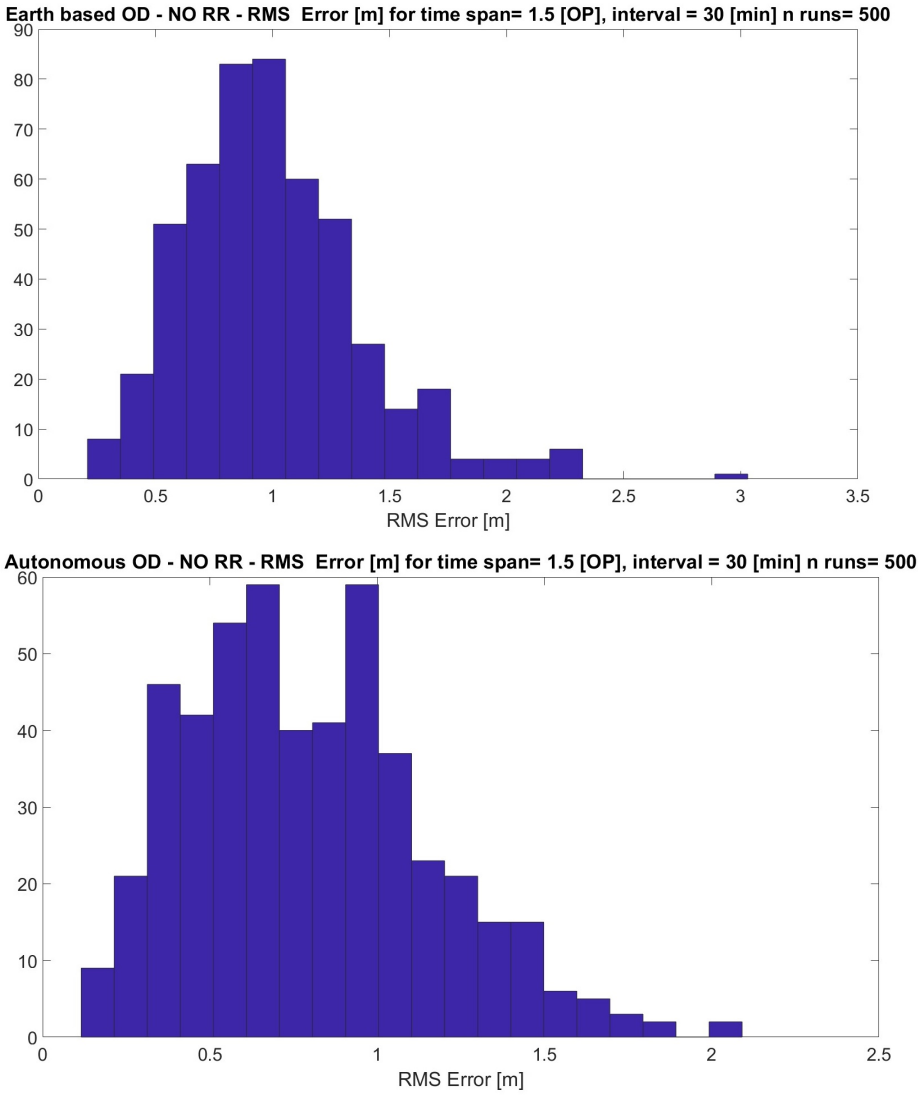

Figure 8. Histograms for the rms orbit error with 500 Monte Carlo runs, using only range measures, (**top**) Earth-based OD, (**bottom**) Autonomous OD.

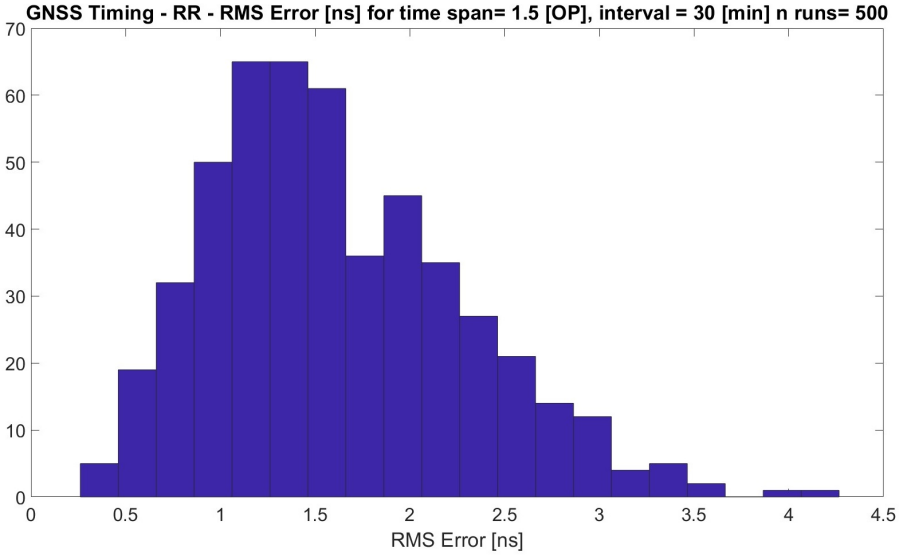

Figure 9. *Cont.*

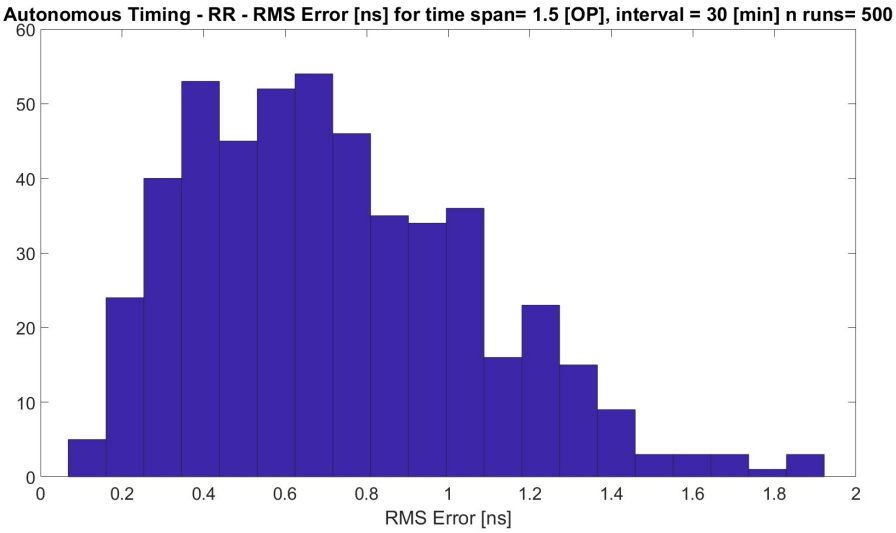

Figure 9. Histograms for the RMS timing error with 500 Monte Carlo runs, using range and range-rate measures, (**top**) GNSS timing, (**bottom**) Autonomous timing.

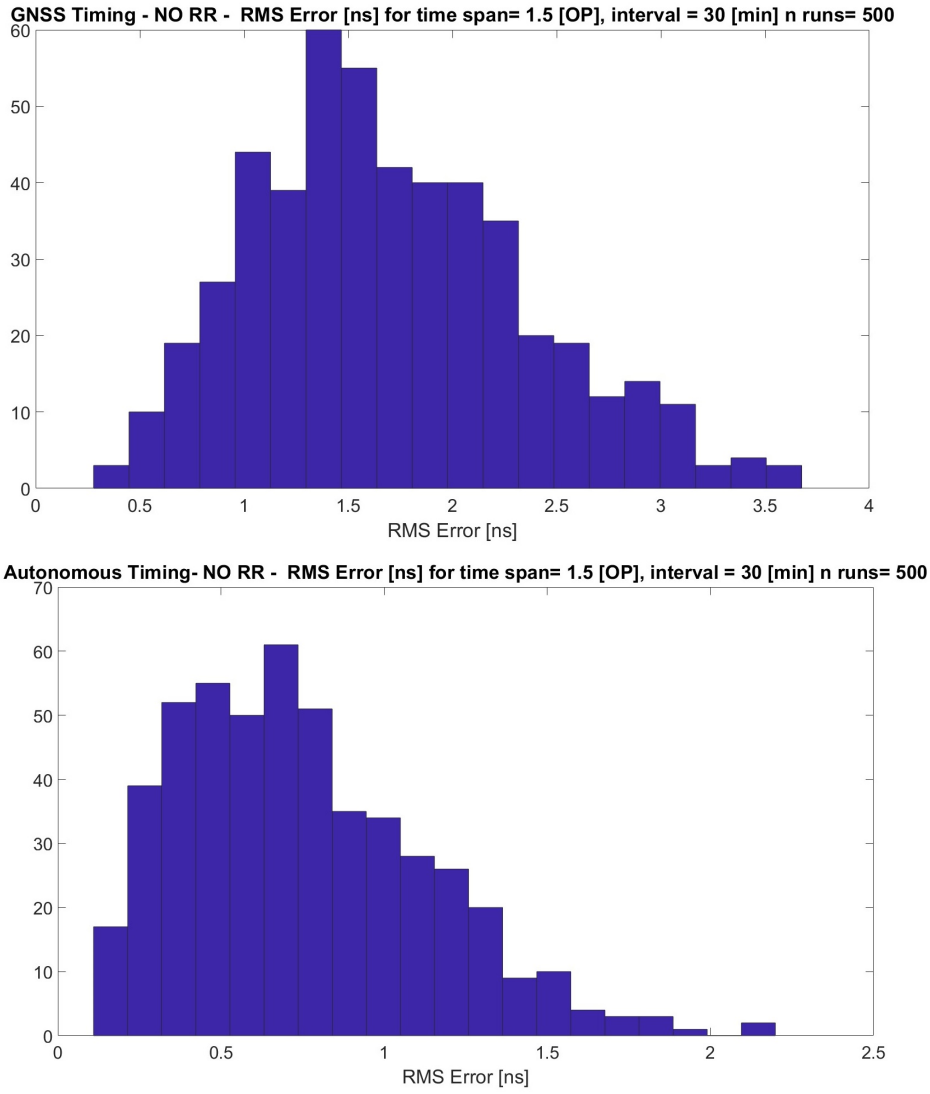

Figure 10. Histograms for the rms timing error with 500 Monte Carlo runs, using only range measures, (**top**) GNSS timing, (**bottom**) Autonomous timing.

In Table 4, more results for the different measurement rates are reported. As before, the 90th percentile of the RMS error obtained for each run on 500 runs is reported for both cases and using the GNSS satellite or the, here proposed, autonomous solution.

Table 4. 90th percentile of the RMS error for the Satellite Time Bias (in nanoseconds) for different measurement rates int and measurement time span, T_s, of 3 h.

Earth Based GNSS Timing RMS Error in ns (90th Percentile)						
	NORR			**RR**		
int/T_s	**15 min.**	**30 min.**	**60 min.**	**15 min.**	**30 min.**	**60 min.**
3 h	2.67	2.63	2.67	2.51	2.53	2.55
Autonomous Timing RMS Error in ns (90th Percentile)						
	NORR			**RR**		
int/T_s	**15 min.**	**30 min.**	**60 min.**	**15 min.**	**30 min.**	**60 min.**
3 h	0.88	1.27	1.76	0.93	1.22	1.60

These results show that, without the need for an additional payload for deep-space reception of the GPS signal, it is possible to obtain high synchronization performance for the constellation of NHRO satellites with an RMS error of the order of one nanosecond on a time span of three hours.

6. Conclusions

The results reported in the previous section open the way for various considerations.

First of all, it was demonstrated that the proposed method could be successfully implemented and used in NHRO orbits, leading to precise orbit determination and timing with performances comparable to or better than those obtained by exploiting Earth-based measurement stations. In particular, concerning the case without the use of the range-rate measurements, the results for the autonomous orbit determination are similar to the Earth-based ones for a measurement time span of 9.89 days (1.5 T) and obtain better than the Earth-based if the time span is increased, bounding the 90th percentile of the DRMS errors between 0.32 m and 0.62 m.

On the other hand, in the case of the range and range rate measurements, the results for the autonomous orbit determination are similar to the Earth-based ones starting from a measurement time span of 9.89 days (1.5 T). They remain comparable also for longer time spans, bounding the 90th percentile of the DRMS errors between 0.21 m and 0.43 m.

Last but not least, in many cases, the 90th percentile of the DRMS error of the proposed method is lower than one meter, obtaining ultra-precise orbit parameters for the spacecraft. This consideration is also true in the case of the very simple configuration that does not use the range-rate measurements, allowing for a simplified HW in the anchors. In addition, in this last case, for Time Spans longer than 1.5 T, the performances reach the meter or sub-meter levels.

Concerning the synchronization performance, the proposed method always gives better results than the one proposed in [38] by the same authors. One of the reasons is that, in the proposed method, the timing accuracy does not depend on the spacecraft position accuracy and on the GNSS satellite's position accuracy, moreover, the propagation errors are lower (the range measurement from the GNSS satellite used for time synchronization in [18] depends, for example, also on the ionosphere delay).

Coming to the application, the Lunar orbiting constellation in NHRO, it is possible to assume that the constellation can be used for navigation purposes due to its high OD&T performance also with no or minimal contact with the Earth, assuring an autonomous navigation service to other spacecraft and rovers. This is an important result because, as mentioned before, in the future, the number of missions to be controlled from the Earth will grow, leading to a possible capacity limit of the terrestrial Deep Space Network. Having

the possibility to provide an autonomous and independent navigation service on the Moon by exploiting a small constellation of spacecraft will overcome this limit.

Moreover, these autonomous properties can be much more useful for future missions to other planets, such as those for Mars exploration and colonization, just because, as the spacecraft gets further away, it becomes more difficult to perform the OD&T from Earth.

Last but not least is some consideration about the limit of the proposed approach. It must be recalled that at least two important hypotheses carried out in this work may be considered as potential drawbacks.

First, the main spacecraft must have the ability to solve the orbit determination problem, accumulating measurements for a long period (comparable with the orbiting period on the Halo orbit) and with a high rate of measurements (on the order of hours or fraction of hour depending on the selected configuration). In the author's opinion, for the proposed test case and many other future missions, this is not a real limit just because it is related to the HW and SW capability (i.e., storage memory and processing power on board that are always improving with time following, for example, the Moore law [39]). Moreover, in the specific case of the here proposed application, it is based on the Gateway, which will be able to carry all the processing and storing facilities needed because it will be a space-station designed for humans and space laboratories.

The second possible limit is due to the gravitational model used. The Circular Restricted Three-Body used here does not take into account perturbations such as, for example, the perturbation of gravitational fields for the two celestial bodies, or the effects of other deep space celestial bodies, or solar radiation pressure. These perturbations were not added to keep the method formulation as general as possible and applicable to any possible system of three bodies, postponing the introduction of the perturbations for more precise evaluation for specific cases and for the different possible solutions or applications. However, the used model is the same for the two scenarios compared in the paper, leading to the same limitation in both the methods and, in the author's opinion, it is enough for a first comparison of the performances. Moreover, if the specific applications or spacecraft limitations will not allow the introduction of a more complex model that also include the most important perturbations, another approach can also be attempted: a time-by-time Earth-based calibration procedure, by exploiting the Earth-based Deep Space Network that, in any case, must be used for periodical Command and Control purposes.

Author Contributions: Conceptualization, G.S. and M.L.; Formal analysis, G.S. and M.L.; Methodology, G.S. and M.L.; Validation, G.S. and M.L.; Writing—original draft, G.S. and M.L.; Writing—review and editing, G.S. All authors have read and agreed to the published version of the manuscript.

Funding: This research received no external funding.

Data Availability Statement: Not applicable.

Conflicts of Interest: The authors declare no conflict of interest.

References

1. NASA. *Webb Arrives in Orbit of L2, Teams Look Ahead to Five Months of Commissioning*; NASA: Washington, DC, USA, 2022.
2. Blanc, M.; Mandt, K.E.; Mousis, O.; André, N.; Bouquet, A.; Charnoz, S.; Craft, K.L.; Deleuil, M.; Griton, L.; Helled, R.; et al. Science Goals and Mission Objectives for the Future Exploration of Ice Giants Systems: A Horizon 2061 Perspective. *Space Sci. Rev.* **2020**, *217*, 1–59. [CrossRef]
3. Grebow, D.J.; Ozimek, M.T.; Howell, K.C.; Folta, D.C. Multibody Orbit Architectures for Lunar South Pole Coverage. *J. Spacecr. Rocket.* **2008**, *45*, 344–358. [CrossRef]
4. Hamera, K.E.; Mosher, T.J.; Gefreh, M.A.; Paul, R.; Slavkin, L.; Trojan, J. An Evolvable Lunar Communication and Navigation Constellation Concept. In Proceedings of the 2008 IEEE Aerospace Conference, Big Sky, MT, USA, 1–8 March 2008; pp. 1–20.
5. Romagnoli, D.; Circi, C. Lissajous trajectories for lunar global positioning and communication systems. *Celest. Mech. Dyn. Astron.* **2010**, *107*, 409–425. [CrossRef]
6. Circi, C.; Romagnoli, D.; Fumenti, F. Halo orbit dynamics and properties for a lunar global positioning system design. *Mon. Not. R. Astron. Soc.* **2014**, *442*, 3511–3527. [CrossRef]
7. Hill, K. Autonomous Navigation in Libration Point Orbits. Ph.D. Thesis, The Colorado Center for Astrodynamics Research, University of Colorado, Boulder, CO, USA, 2007.

8. NASA. *NASA Lunar Gateway*; NASA: Washington, DC, USA, 2022.
9. Bardan, R.N. CAPSTONE Forges New Path for NASA's Future Artemis Moon Missions; NASA: Washington, DC, USA, 2022.
10. Leonardi, M.; Sirbu, G.; Stallo, C.; Eleuteri, M.; Lauro, C.D.; Iannone, C.; Zoppo, E.D. Autonomous Lunar Satellite Navigation System: Preliminary Performance Assessment on South Pole. In Proceedings of the 2021 International Technical Meeting of the Institute of Navigation, Online, 25–28 January 2021. [CrossRef]
11. Sirbu, G.; Leonardi, M.; Carosi, M.; Di Lauro, C.; Stallo, C. Performance evaluation of a lunar navigation system exploiting four satellites in ELFO orbits. In Proceedings of the 2022 IEEE 9th International Workshop on Metrology for AeroSpace (MetroAeroSpace), Pisa, Italy, 27–29 June 2022; pp. 146–151. [CrossRef]
12. *Recommendation for Space Data System Standards Pseudo-Noise (PN) Ranging Systems Recommended Standard CCSDS 414.1-B-2 Blue Book*; Technical Report; Council of the Consultative Committee for Space Data Systems (CCSDS): Washington, DC, USA, 2014.
13. Andrews, K.S.; Hamkins, J.; Shambayati, S.; Vilnrotter, V.A. Telemetry-based ranging. In Proceedings of the 2010 IEEE Aerospace Conference, Big Sky, MT, USA, 6–13 March 2010; pp. 1–16.
14. Hamkins, J.; Kinman, P.W.; Xie, H.; Vilnrotter, V.A.; Dolinar, S. *Telemetry Ranging: Concepts*; NASA: Washington, DC, USA, 2015.
15. *Proximity-1 Space Link Protocol - Physical Layer Ccsds 211.1-b-4*; Technical Report: Council of the Consultative Committee for Space Data Systems (CCSDS): Washington, DC, USA, 2013.
16. Woo, S.S.; Gao, J.L.; Mills, D.L. Space Network Time Distribution and Synchronization Protocol Development for Mars Proximity Link. In Proceedings of the SpaceOps 2010 Conference Delivering on the Dream Hosted by NASA Marshall Space Flight Center and Organized by AIAA, Huntsville, Alabama, 25–30 April 2010.
17. Mazarico, E.M.; Sun, X.; Torre, J.M.; Courde, C.; Chabé, J.; Aimar, M.; Mariey, H.; Maurice, N.; Barker, M.K.; Mao, D.; et al. First two-way laser ranging to a lunar orbiter: Infrared observations from the Grasse station to LRO's retro-reflector array. *Earth Planets Space* **2020**, *72*, 1–14. [CrossRef]
18. Kaplan, E.; Hegarty, C.J. *Understanding GPS/GNSS: Principles and Applications*, 3rd ed.; Artech House, Inc.: Norwood, MA, USA, 2017.
19. Poisel, R. *Electronic Warfare Target Location Methods*, 2nd ed.; Artech House Radar Library, Artech House: Norwood, MA, USA, 2012.
20. Sokolova, N. Doppler Measurements and Velocity Estimation: Comparison of Standard and High Sensitivity Receivers. Master's Thesis, Department of Geomatics Engineering, The University of Calgary, Calgary, AB, Canada, 2009.
21. Yu, F.; He, Z.; Xu, N. Autonomous navigation for GPS using inter-satellite ranging and relative direction measurements. *Acta Astronaut.* **2019**, *160*, 646–655. [CrossRef]
22. Ming Mo, S.; Jun Jin, X.; Lin, C.; Zhang, W.; Xu, Z.; He Jin, Z. Multi-Satellite Relative Navigation Scheme for Microsatellites Using Inter-Satellite Radio Frequency Measurements. *Sensors* **2021**, *21*, 3725. [CrossRef] [PubMed]
23. Ma, H.J.; Wu, H.; Wu, J.F.; Li, M.; Wang, K.; He, Z.; Zhao, D. Design and implementation of dual one-way precise ranging and time synchronization system. In Proceedings of the 2013 Joint European Frequency and Time Forum & International Frequency Control Symposium (EFTF/IFC), Prague, Czech Republic, 21–25 July 2013; pp. 831–834.
24. Qin, T.; Qiao, D.; Macdonald, M. Relative Orbit Determination Using Only Intersatellite Range Measurements. *J. Guid. Control Dyn.* **2019**, *42*, 703–710. [CrossRef]
25. Su, X.; Geng, T.; Li, W.; Zhao, Q.; Xie, X. Chang'E-5T Orbit Determination Using Onboard GPS Observations. *Sensors* **2017**, *17*, 1260. [CrossRef]
26. Gao, Z.; Hou, X.Y. Comparison of Autonomous Orbit Determination for Satellite Pairs in Lunar Halo and Distant Retrograde Orbits. *NAVIGATION J. Inst. Navig.* **2022**, *69*, navi.522. [CrossRef]
27. Ming Mo, S.; Jun Jin, X.; Hu, W.; Zhang, W.; Xu, Z.; He Jin, Z. Distributed multi-satellite measurement scheme oriented towards microsatellite formations. *Electron. Lett.* **2020**, *56*, 252–255.
28. Molli, S.; Durante, D.; Boscagli, G.; Cascioli, G.; Racioppa, P.; Alessi, E.; Simonetti, S.; Vigna, L.; Iess, L. Design and performance of a Martian autonomous navigation system based on a smallsat constellation. *Acta Astronaut.* **2023**, *203*, 112–124. [CrossRef]
29. *The Future Lunar Communications Architecture*; Report; Interagency Operations Advisory Group, Lunar Communications Architecture Working Group, 2020. Available online: https://www.ioag.org/Public%20Documents/Lunar%20communications%20architecture%20study%20report%20FINAL%20v1.3.pdf (accessed on 10 January 2023).
30. Tapley, B.D.; Schutz, B.E.; Born, G.H. *Statistical Orbit Determination*; Elsevier: Amsterdam, The Netherlands, 2004.
31. Galleani, L.; Sacerdote, L.; Tavella, P.; Zucca, C. A mathematical model for the atomic clock error. *Metrologia* **2003**, *40*, S257. [CrossRef]
32. Navipedia-(ESA). "Clock Modelling". 2018. Available online: https://gssc.esa.int/navipedia/index.php/Clock_Modelling (accessed on 10 January 2023).
33. Parkinson, B.W.; Spilker, J.J. *Global Positioning System: Theory and Applications*; American Institute of Aeronautics and Astronautics, Inc.: Reston, VA, USA, 1996.
34. Navipedia-(ESA). "Clock Modelling". 2021. Available online: https://gssc.esa.int/navipedia/index.php/GPS_Navigation_Message (accessed on 10 January 2023).
35. NASA. *A Lunar Orbit That's Just Right for the International Gateway*; NASA: Washington, DC, USA, 2022.
36. NASA's Lunar Exploration Program Overview. 2020. Available online: https://www.nasa.gov/sites/default/files/atoms/files/artemis_plan-20200921.pdf (accessed on 20 December 2022).

37. Tanaka, T.; Ebinuma, T.; Nakasuka, S.; Malki, H.A. A Comparative Analysis of Multi-Epoch Double-Differenced Pseudorange Observation and Other Dual-Satellite Lunar Global Navigation Systems. *Aerospace* **2021**, *8*, 191. [CrossRef]
38. Leonardi, M.; Sirbu, G.; Rana, N.; De Angeli, E.; Eleuteri, M. Lunar Gateway Autonomous Orbit Determination and Time Synchronization by the use of one or two small orbiters. In Proceedings of the 2022 73rd International Astronautical Congress (IAC), Paris, France, 18–22 September 2022; International Astronautical Federation (IAF): Paris, France, 2022.
39. Moore, G.E. Cramming more components onto integrated circuits, Reprinted from Electronics, volume 38, number 8, April 19, 1965, pp.114 ff. *IEEE Solid-State Circuits Newsl.* **2006**, *20*, 33–35. [CrossRef]